HHS Public Access

Author manuscript

Cancer Res. Author manuscript; available in PMC 2020 February 01.

Published in final edited form as:

Cancer Res. 2019 February 01; 79(3): 482–494. doi:10.1158/0008-5472.CAN-18-1214.

Tet2-dependent Hydroxymethylome Plasticity Reduces Melanoma Initiation and Progression

Elise Bonvin[1], **Enrico Radaelli**[2,3], **Martin Bizet**[1], **Flavie Luciani**[4,5], **Emilie Calonne**[1], **Pascale Putmans**[1], **David Nittner**[4,5,6], **Nitesh Kumar Singh**[1], **Sara Francesca Santagostino**[7,8], **Valérie Petit**[9], **Lionel Larue**[9], **Jean Christophe Marine**[4,5], and **François Fuks**[1]

[1]Laboratory of Cancer Epigenetics, Faculty of Medicine, ULB-Cancer Research Center (U-CRC), Université Libre de Bruxelles (ULB), Brussels, Belgium.

[2]Mouse Histopathology Core Facility, VIB Center for Brain & Disease Research, Leuven, Belgium.

[3]Comparative Pathology Core, University of Pennsylvania, School of Veterinary Medicine, Department of Pathobiology, Philadelphia, Pennsylvania.

[4]Laboratory for Molecular Cancer Biology, VIB Center for Cancer Biology, Leuven, Belgium.

[5]Laboratory for Molecular Cancer Biology, Department of Oncology, KU Leuven, Leuven, Belgium.

[6]Histopathology Expertise Center, VIBKU Leuven Center for Cancer Biology, Leuven, Belgium.

[7]Laboratory of Comparative Pathology, Memorial Sloan Kettering Cancer Center, The Rockefeller University, Weill Cornell Medicine, New York, New York.

[8]Department of Safety Assessment, Genentech, Inc., South San Francisco, California.

[9]Normal and Pathological Development of Melanocytes, CNRS UMR3347, INSERM U1021, Institut Curie, Orsay, France.

Abstract

Although numerous epigenetic aberrancies accumulate in melanoma, their contribution to initiation and progression remain unclear. The epigenetic mark 5-hydroxymethylcyto-sine (5hmC),

Corresponding Authors: François Fuks, Free University of Brussels, Route de Lennik 808, Brussels 1070, Belgium. Phone: 322-555-6245; Fax: 322-555-6257; ffuks@ulb.ac.be; and Jean Christophe Marine, Phone: 321-633-0368; JeanChristophe.Marine@kuleuven.vib.be.

Authors' Contributions

Conception and design: E. Bonvin, J.C. Marine, F. Fuks

Development of methodology: E. Bonvin, E. Radaelli, F. Luciani, E. Calonne, P. Putmans

Acquisition of data (provided animals, acquired and managed patients, provided facilities, etc.): E. Bonvin, E. Radaelli, F. Luciani, P. Putmans, D. Nittner, V. Petit, L. Larue

Analysis and interpretation of data (e.g., statistical analysis, biostatistics, computational analysis): E. Bonvin, E. Radaelli, M. Bizet, P. Putmans, N.K. Singh, S.F. Santagostino, L. Larue, J.C. Marine, F. Fuks

Writing, review, and/or revision of the manuscript: E. Bonvin, E. Radaelli, S.F. Santagostino, L. Larue, J.C. Marine, F. Fuks

Administrative, technical, or material support (i.e., reporting or organizing data, constructing databases): E. Bonvin, E. Radaelli, P. Putmans

Study supervision: E. Bonvin, J.C. Marine, F. Fuks

Note: Supplementary data for this article are available at Cancer Research Online (http://cancerres.aacrjournals.org/).

Disclosure of Potential Conflicts of Interest

No potential conflicts of interest were disclosed.

generated through TET-mediated DNA modification, is now referred to as the sixth base of DNA and has recently been reported as a potential biomarker for multiple types of cancer. Loss of 5hmC is an epigenetic hallmark of melanoma, but whether a decrease in 5hmc levels contributes directly to pathogenesis or whether it merely results from disease progression–associated epigenetic remodeling remains to be established. Here, we show that NRAS-driven melanomagenesis in mice is accompanied by an overall decrease in 5hmC and specific 5hmC gains in selected gene bodies. Strikingly, genetic ablation of Tet2 in mice cooperated with oncogenic NRASQ61K to promote melanoma initiation while suppressing specific gains in 5hmC. We conclude that Tet2 acts as a barrier to melanoma initiation and progression, partly by promoting 5hmC gains in specific gene bodies.

Introduction

Disruption of the balance of epigenetic networks has been causally linked to several pathologies, including cancer. 5-Methylcytosine (5mC) in DNA is one of the most extensively studied epigenetic modifications in the mammalian genome. Cancer cells display highly dysregulated DNA methylation profiles, often characterized by global hypomethylation combined with hypermethylation of promoter CpG islands (CGI). These anomalies presumably lead to genome instability and aberrant expression of tumor suppressor genes or oncogenes. The Ten-Eleven-Translocation (TET) enzyme family has three members: *TET1*, *TET2*, and *TET3*. These proteins are 2-oxoglutarate-, oxygen-, and iron-dependent dioxygenases catalyzing the oxidation of 5-mC to 5-hydroxymethylcytosine (5hmC). They have been identified as key players in cytosine demethylation (1) and in the control of cell differentiation and transformation (2–5). Metabolic perturbations due to mutations in the genes encoding isocitrate dehydrogenase (IDH), fumarate hydratase (FH), or succinate dehydrogenase (SDH) also inhibit the TET enzymes and, in turn, DNA demethylation.

Malignant melanoma, the deadliest form of skin cancer, is a complex disease influenced by genetic and epigenetic factors (6–9). Relevant epigenetic alterations include, among others, promoter hypermethylation and silencing of the $p16^{ink4a}$ or *Pten* tumor suppressor genes (10, 11), silencing of the TGFβ pathway via acquisition of repressive chromatin marks (12), and increased expression of the cancer-associated chromatin methyltransferase Ezh2 (9). In human melanoma and in several other cancer types, levels both of the TET enzymes and of the product of their activity (DNA 5hmC) are substantially lower than in normal tissue (13, 14). Although *Tet2*-inactivating mutations are common driver mutations in hematopoietic malignancies, only a negligible fraction of human melanomas exhibit such mutations. Similarly, mutations in other components of the 5hmC-generating enzyme machinery (i.e., other *Tet* genes and *Idh* genes) are also very rare in melanoma clinical samples (15, 16). The molecular mechanisms underlying the global loss of 5hmC during melanoma progression thus remain to be elucidated. In fact, it remains to be established whether this loss contributes directly to melanoma initiation and/or progression. To address this, we genetically ablated *Tet2* in a well-defined NRAS-driven murine melanoma model. This approach allowed us to establish a clear genetic and causal link between Tet2 and

melanomagenesis, and to gain insights into the mechanism of Tet2-mediated tumor suppression.

Materials and Methods

Transgenic mice

Tyr::NRas$^{Q61K/°}$ (MGI:3768645), *Ink4a–Arf* knockout, *Tyr::Cre* (MGI:3573938), and *Tet2*$^{lox/lox}$ mice have been described previously (3, 17–19). Transgenic mice with the abovementioned genotypes were crossed to generate our *Tyr::NRas*$^{Q61K/°}$; Ink4$^{-/-}$; *Tyr::Cre;* *Tet2*$^{lox/lox}$ and *Tet2*$^{+/+}$ mice of interest. The resulting mice had a mixed genetic background consisting primarily of C57BL/6J (over 85%) and, to a much lesser extent, 129/SvEv, DBA/2. For genotyping, genomic DNA was prepared from ear skin biopsies and analyzed by PCR with the following primers: *Tet2* (Fwd: AAGAATTGCTACAGGCCTGC; Rev: TTCTTTAGCCCTTGCTGAGC; LoxP3R: TAGAGGGAGGGGGCATAAGT), *Tyr::Cre* (Fwd: GTCACTCCAGGGGTTGCTGG; Rev: CCGCCGCATAACCAGTGA), *Ink4a* (fwd: GCAGTGTTGCAGTTTGAACCC; Rev: GTGGCAACTGATTCAGTTGG) as described in the original papers. Mice were kept in accordance with the institutional guidelines regarding the care and use of laboratory animals, and all procedures were approved by the Institutional Ethics Committee (Agreement: LA1230572). The mice were evaluated two to three times per week for tumor appearance and progression. They were killed as soon as the tumors reached 1 cm^3 or sooner if they were showing any signs of suffering. Those that did not develop melanoma were sacrificed if they showed any clinical signs of suffering (such as a weight loss exceeding 20% of the total body weight), which were mainly related to advanced age. Melanoma-free survival graphs were drawn with the free-access tool KmWin (20). Following euthanasia, a complete postmortem examination was performed, and all organs were macroscopically inspected and dissected. Lesions that were not clinically apparent because they affected internal organs, including enlarged lymph nodes and organs with space-occupying lesions, were harvested along with the more obvious primary cutaneous melanomas and control nevi.

Biospies were snap-frozen in liquid nitrogen for further analysis or fixed in 4% paraformaldehyde, processed, and embedded in paraffin for histologic studies.

Histopathologic analyses, pathology descriptions, and diagnoses were performed for all lesions detected on H&E-stained paraffin sections. Melanocytic skin lesions were grouped into four main types according to Campagne and colleagues (21). Briefly, the types ranged from benign lesions (types A and B) to malignant lesions (melanoma, type D), with an intermediate category comprising melanocytic lesions of unknown malignant potential (atypical nevus, type C). The ratio of the number of events to the number of examined skin biopsies was calculated. Distant metastases and lymph nodes bearing melanocytic lesions were also recorded.

DNA preparation

The QIAamp DNA Mini Kit (Qiagen) was used to extract Genomic DNA from biopsies of melanomas and nevi according to the manufacturer's protocol. DNA concentration was measured with a NanoDrop spectrophotometer.

Analysis of global 5hmC and mC levels by mass spectrometry (LC/MS-MS)

Genomic DNA (1 μg) was incubated with 5 U of DNA Degradase Plus (Zymo Research) at 37°C for 3 hours. The resulting mixture of 2′-deoxynucleosides was analyzed on a Triple Quad 6500 mass spectrometer (AB Sciex) fitted with an Infinity 1290 LC system (Agilent) and an Acquity UPLC HSS T3 column (Waters). The eluent was a gradient of water and acetonitrile with 0.1% formic acid. External calibration was performed with synthetic standards, and for accurate quantification, all samples and standards were spiked with isotopically labeled nucleosides. Levels of 5hmC and mC are expressed as a percentage of total cytosines.

Genome-wide 5hmC profiling (hMeDIP-Seq)

Genomic DNA (1 μg) was diluted in ultra-pure water to 35 ng/μL and then sonicated in cold water with a Bioruptor sonicator (Diagenode) to obtain fragments averaging 300 bp in size. The fragmented DNA was used in combination with a Hydroxymethyl Collector (Active Motif) according to the manufacturer's protocol. Briefly, a glucose moiety containing a reactive azide group was enzymatically linked to hydroxymethylcytosine in DNA, creating glucosyl-hydroxymethylcytosine. Next, a biotinconjugate was chemically attached to the modified glucose via a "click reaction", and magnetic streptavidin beads were used to capture the biotinylated-5hmC DNA fragments. After extensive washing steps and chemical elution, the hydroxymethylated DNA fragments released from the beads were used in sequencing experiments.

Library preparation was performed with the TruSeq ChIP Sample Prep Kit (Illumina). Briefly, double-stranded DNA was subjected to 5′ and 3′ protruding end repair and nontemplated adenines were added to the 3′ ends of the blunted DNA fragments to allow ligation of Illumina multiplex adapters. DNA fragments were then size selected (300–500 bp) to remove all nonligated adapters. Eighteen PCR cycles were carried out to amplify the library, which was then quantified by fluorometry with Qubit 2.0. The integrity of the library was assessed with a 2100 Bioanalyzer (Agilent) before sequencing with the Illumina NextSeq500 sequencer.

The BWA software was then used to map sequencing reads to the mouse genome (NCBI Build 37/UCSC hg19; ref. 22). Raw data are available in the Gene Expression Omnibus database. Read density was computed by counting the reads in nonoverlapping 2-kb windows tiling the whole genome thanks to the "feature-Counts" software (23). Reads mapping to multiple locations in the reference genome or overlapping two windows were divided among their associated windows. Windows presenting a significantly different 5hmC level between tumor samples and nevi were identified with edgeR software (log fold change > 1.5 and FDR < 0.05; ref. 24).

For annotation purposes, enhancers were obtained from the Enhancer VISTA database (https://enhancer.lbl.gov/; downloaded on January 18, 2016; ref. 25) and lifted to mm10 genome with the liftOver tool from UCSC, gene bodies were defined as regions from the TSS to the TTS of RefSeq genes (downloaded from UCSC on March 6, 2017), while promoters ranged from −2 kb to the TSS, CGI positions were obtained from UCSC (downloaded on March 6, 2017), and shores were defined as regions surrounding CGIs by up to 2 kb. All windows were annotated by comparing window center genomic positions with the positions of the aforementioned features, using bedtools annotate (26). Read densities shown in the different figures were normalized to the total number of reads and expressed in $\log_2$ counts per million ($\log_2$ CPM).

hMeDIP-Seq targets validation

DNA samples were prepared as for hMedIP-seq and 1 pg of 550 bp of human *Son* gene PCR product containing hmC (100% of C was hmC) was added per microgram of fragmented melanoma DNA or nevus DNA for normalization procedure. Pull-down of 5hmC was performed as described above on both the samples and a negative control (pull-down negative: no containing β-glucosyltransferase enzyme), and the recovered DNA was diluted five times prior to analysis. PCR were run on selected positive and negative DhmRs. Cp values were normalized to Input. Fold changes were calculated for pull-down values over pull-down negative control and ratio were normalized to spike in values. Primers are listed in Supplementary Fig. S4B.

RNA analysis

RNA preparation.—Total RNA was extracted from melanoma biopsies and nevi with the RNeasy Kit (Qiagen). DNase treatment was performed with the DNA-free DNase Kit (Ambion) according to the manufacturer's instructions. RNA concentration was measured with NanoDrop or Qubit. RNA quality was determined with a bioanalyzer and considered suitable for further experiments when the RIN reached at least 8.

Gene expression_RT-PCR/QPCR.—SuperScript II reverse transcriptase (Invitrogen) was used according to the manufacturer's protocol to synthesize cDNA from 1 μg total RNA in combination with random hexamers. The cDNA was then used as template for qRT-PCR based on SYBR Green detection with the Light Cycler 480 (LC480) system (Roche). Relative expression was determined by the $\Delta\Delta C_t$ method using the *Actin, Sdha, Gapdh*, and *Hprt* genes as controls for normalization. The PCR primers used for amplification are listed in Supplementary Fig. S2.

RNA-seq.—Following RNA isolation (described above), RNA quality was assessed with a Bioanalyzer (Agilent) and the library was constructed with 1 μg total RNA and Illumina TruSeq Stranded Total RNA Ribo-Zero H/M/R Gold (Illumina, RS-122–2301) according to the manufacturer's instructions. Libraries were quantified with a Bioanalyzer (Agilent) and Qubit 2.0 and sequenced on an Illumina NextSeq 500 instrument to a depth of at least 18 million reads, a 75-bp single read. The reads were mapped to the mouse genome with mm10 reference assembly from UCSC (https://genome.ucsc.edu/), using STAR (27). Reads mapped to genes were counted with HTSeq-count (28), using the union–intersection mode

and refSeq mm10 transcriptome annotations from UCSC. Duplicate reads mapping to the same location were removed with Picard (http://broadinstitute.github.io/picard). Differential expression analysis was performed with edgeR (24). A gene was considered differentially expressed when the absolute fold change was above 2 and FDR < 0.05. A PCA plot was generated on the regularized $\log_2$ transformed (rlog_2) read count data for all the samples. rlog_2 was performed with the DESeq2 package (29) of Bioconductor, and the PCA plot was generated with the ggplot2 package.

In silico cross-comparisons

Venn diagrams were drawn with a free-access tool (http://www.biovenn.nl/index.php).

Searching for *cis*-regulatory elements in our 5hmC data set was done with the free-access tool i-Cis Target (https://gbiomed.kuleuven.be/apps/lcb/i-cisTarget/).

Gene ontology analysis

Ingenuity Pathway Analysis (IPA) software with the default parameters was used for core analysis.

Primary melanocyte cultures

Skin explants from 1-year-old mice *Tyr::NRas*^{Q61K}; Ink4$^{-/-}$; *Tyr::Cre; Tet2*$^{lox/lox}$ and *Tyr::NRas*^{Q61K}; Ink4$^{-/-}$; *Tyr::Cre; Tet2*$^{+/+}$ mice were trypsinized overnight. The next day, the epidermis was ripped off, cut into small pieces, and put into Melanocyte Growth Medium 4 (Lonza) at 37°C, 5% CO_2 in a humidified incubator until melanocytes expanded and detached from the explant.

Protein lysates and Western blotting

Cultured primary melanocytes were lysed at 4°C in cell lysis buffer (50 mmol/L Tris pH 8.0, 150 mmol/L NaCl, 50 mmol/L EDTA, 0.5% NP-40) supplemented with a protease inhibitor cocktail (Roche). After SDS-PAGE, lysates were transferred to PVDF membranes (Millipore). Membrane blocking (5% milk in TBS, 0.2% Tween-20) was followed by incubation with the appropriate primary antibodies and HRP-conjugated secondary antibody (Cell Signaling Technology). Proteins were detected with the ECL substrate or the SuperSignal West Pico Chemiluminescent Substrate (Thermo Fisher Scientific). The primary antibodies used were as follows: anti-ERK2 (Santa Cruz Biotechnology Inc.), anti–p-ERk, anti–phospho-Akt (Ser473), anti-Akt (Cell Signaling Technology), anti-cyclin A (Santa Cruz Biotechnology), anti-PCNA (Abcam), and anti-actin (Sigma).

Results

DNA 5hmC landscape remodeling in spontaneous NRAS-driven melanoma

Upregulation of the rat sarcoma protein/raf protooncogene serine threonine protein kinase/mitogenactivated protein kinase kinase/extracellular signalregulated kinase (RAS/RAF/MEK/ERK) pathway has emerged as an obligate event in the etiology of a large majority of melanomas. In human, activating mutations in *BRAF* (51%–63%) and *NRAS* (21%–28%) are mutually exclusive and, together, account for as many as 75% to 80% of

melanomas. Although loss of 5hmC has been described in human melanoma (15), whether there exists a causal link between this loss and melanoma pathogenesis remains unclear. To address this question, we were free to choose between two well-established mouse models of spontaneous melanoma: a *Braf* mutation–driven or a *Nras* mutation–driven model. We chose the latter (30). In contrast to human cutaneous melanoma, which displays a highly altered genome architecture with a high DNA mutation burden, the $Nras^{Q61K}$-driven melanoma mouse model appears genetically stable (31) and is therefore well suited for dissecting the roles of specific genetic alterations in melanomagenesis.

Transgenic mice expressing the mutated Nras oncogene in the melanocyte compartment (*Tyr::*$Nras^{Q61K}$) exhibit hyperpigmented skin and eventually develop spontaneous cutaneous melanoma (Fig. 1A), as described previously (30). The long latency of tumor development indicates that additional genetic and/or epigenetic events are required for full-blown tumorigenesis in this model. Macroscopic examination revealed that tumors arose on the hairy parts of the bodies of the mutant mice, mainly on the back and neck. Biopsies of skin and tumors from mice of both genders were subjected to histologic analyses to confirm their melanocytic origin. Skin biopsies from *Tyr:: Nras*^{Q61K} mice, diagnosed as benign melanocytic proliferations of the (ML)-A (classical nevus) or (ML)-B (cellular nevus) type, are hereafter simply called “nevi.” Malignant melanocytic proliferations were defined as either (ML)-C or (ML)-D for atypical nevus and melanoma, respectively (Supplementary Fig. S1).

Consistently with the observed loss of 5hmC in human melanoma (15), mass spectrometry assessment of the global 5hmC content showed a striking depletion of this DNA mark in melanoma biopsies compared with control nevi (Fig. 1B). In contrast, we observed no significant decrease in 5mC in melanoma samples as compared with nevi (Supplementary Fig. S2).

Unexpectedly, although a clear overall decrease in 5hmC was observed, careful examination of the genome-wide distribution of 5hmC, based on a barcoded hydroxymethylated DNA collection approach coupled with deep sequencing (hMeDIP-seq), revealed an enrichment in 5hmC at discrete loci in the melanoma samples (Supplementary Table S1). Accordingly, supervised hierarchical clustering of the 5hmC distribution identified nevi and melanomas as two distinct entities (Fig. 1C). As previously described, 5hmC was mainly associated with gene-rich regions and absent from transcription start sites (or TSS) in both control nevus samples and melanoma samples (32). Compared with nevi, a total of 2,022 DNA regions in melanoma samples showed significant differential enrichment in 5hmC (fold change > 2 and FDR < 0.05) and were called differentially hydroxymethylated regions (DhmR). A large proportion of DhmRs tended to gain hmC and this occurred mainly in gene bodies (Fig. 1D and E). To check the reliability of our hmedIP-seq approach, we repeated the hmC pull-down on a few randomly chosen melanomas and nevi from the same batch of samples and included an hmC spike for better normalization. The same amount of hmC spike was added to all samples, pull-down was performed following the exact same protocol as for hmedIP-seq, and DNA containing hmC was determined by qPCR. Primers targeting hmedIP-positive and -negative regions were chosen randomly and although the range of fold change between tumors and nevi could vary between the two different experiments, we were able to validate

the tested DhmRs (Supplementary Fig. S1). Thus, although a global loss of 5hmC was observed in spontaneous mouse melanoma lesions, several loci exhibited increased hydroxymethylation. This observation is in keeping with recent data showing local elevation of 5hmC in pancreatic cancer samples (33).

Gene ontology analysis revealed an involvement of genes displaying differential 5-hydroxymethylation in "Cancer" (P value between 7.99×10^{-4} and 5.15×10^{-19}) and "dermatological diseases and conditions" (P value between 2.5×10^{-4} and 7.82×10^{-17}). Some of these genes were also linked to pathways involved in "nervous system development and function" (P between 7.99×10^{-4} and 4.59×10^{-12}). To assess whether differential 5-hydroxymethylation correlated with specific changes in gene expression, we determined mRNA levels by RNA sequencing (RNA-seq). Unsupervised hierarchical clustering of nevus and melanoma samples showed two separated groups of samples (Fig. 1F). 4616 transcripts showed differential levels in melanomas as compared with nevi (fold change > 2; FDR > 0.05) (Fig. 1G; Supplementary Table S1). Several melanoma-relevant genes appeared upregulated, including *Mitf* (fc 7.53), *Sox10* (fc = 11.14), and *Tbx2* (fc = 30). IPA revealed a significant enrichment in genes involved in molecular mechanisms of cancer ($P = 4.5 \times 10^{-5}$) and pathways known to play important roles in melanomagenesis, such as Wnt/β-catenin ($P = 9.22 \times 10^{-5}$), or in biological processes regulating cell growth and proliferation (P between 5.97×10^{-3} and 4.86×10^{-7}). In contrast to the previously published human data (15), neither *Idh1/2 nor Tet1/2/3* transcripts appeared significantly dysregulated in the *Tyr::Nras*^{Q61K} tumor samples. This indicates that the global 5hmC loss observed in mouse melanoma samples is not caused only by decreased transcript-level expression of genes encoding factors involved in 5hmC biogenesis. Importantly, the significant overlap between differentially hydroxymethylated and differentially expressed genes concerned 170 genes (P = 4.9e−42; Fig. 1H). Among these, *Pcsk6, Mast4, Smo*, and *Gpr158* are reported to be dysregulated in melanoma and/or to play a key role in melanomagenesis (31, 34–37). In addition, for those 170 genes we observed a positive correlation between hmC content and expression ($r = 0.46$; P = 2.7e−10). Although more than a third of DhmR genes showed a change in gene expression, 96% of the dysregulated genes showed no change in 5hmC. This fact simply supports the reported observation that changes in gene transcription can be poorly linked to changes in DNA demethylation (38–42).

Together, these data indicate that melanoma progression is accompanied by a profound remodeling of the hydroxymethylation landscape, with on the one hand an overall decrease in 5hmC and on the other hand, a gain at specific loci within gene bodies. This unexpected observation raises the possibility that hydroxymethylation rewriting, rather than merely a gradual loss of 5hmC, may modulate melanomagenesis. How these two distinct epigenetic effects influence melanoma initiation and/or progression needs to be fully elucidated.

Tet2 deficiency cooperates with oncogenic NRAS to promote melanomagenesis

The observed increase in 5hmC in specific gene bodies prompted us to postulate that this epigenetic effect might modulate melanomagenesis. Importantly, whereas all three Tet proteins can oxidize 5mC and are expressed in human skin/melanomas, in our murine samples, Tet1 was barely detected (Supplementary Fig. S2). In addition, Tet2 is thought to

play the key role in converting 5mC to 5hmC in gene bodies (5) and has been shown to act as a tumor suppressor in human cancers (15). To test the hypothesis that a 5hmC gain within gene bodies might play a role in melanomagenesis, we used a floxed *Tet2* allele (3) to investigate the impact of decreased *Tet2* gene dosage on the incidence and latency of melanomagenesis in melanoma-prone mice having the *Tyr::Nras*^{Q61K} genetic background. *Tyr::Cre* animals (17, 19, 43, 44) were used to conditionally knock out *Tet2* in the melanocyte lineage. To accelerate melanomagenesis, we also decreased expression of the well-established *p16/Ink4a* melanoma tumor suppressor gene (Fig. 2A). In agreement with previous reports, dilution of p16/Ink4a gene enhanced melanoma incidence and reduced the latency (Supplementary Fig. S2; ref. 18). Note that in the mice used, one or both of the *p16/Ink4a* alleles were inactivated, but *p19/Arf* was not, in contrast to previously used mice where the entire *Cdkn2a* locus (including both genes) was knocked out (19). We thus generated cohorts of mice with the following genotypes: *Tyr::Nras*^{Q61K}; ink4a$^{+/-\text{ or }-/-}$; *Tyr::Cre; Tet2*$^{+/+;lox/+\text{ or }lox/lox}$ (Fig. 2B).

WT-Nras mice lacking *Tet2* (*Tyr::Cre; Tet2*$^{lox/lox}$; *Ink4a*$^{+/-\text{ or }-/-}$) did not develop any melanoma lesions. Hence, loss of *Tet2* in melanocytes is not sufficient to promote melanoma. Strikingly, however, when combined with the presence of oncogenic NRas, loss of *Tet2* significantly increased the incidence of tumor appearance and decreased latency and melanoma-free survival (Fig. 2C and D). Loss of one *Tet2* allele was sufficient to accelerate melanomagenesis in both *Ink4a*$^{+/-}$ and *Ink4a*$^{-/-}$ mice. *Tet2* thus functions as a haploinsufficient tumor suppressor gene in melanoma. The percentage of mice developing at least one melanoma lesion was dramatically increased (from 36% to 55%) upon deletion of *Tet2* on the *Ink4*$^{-/-}$ background. The incidence was even higher (78%) upon *Tet2* deletion on the *Ink4*$^{-/-}$ background (Fig. 2D, top). *Tet2* deletion increased the number of melanoma-bearing mice and drastically lowered the average age of tumor appearance, which dropped from 77.5 ± 9.7 to 50.5 ± 9.7 weeks in mice with the *Ink4*$^{+/-}$ background and from 61.5 ± 12 to 40.5 ± 10.4 weeks in mice with the *Ink4*$^{-/-}$ background (Fig. 2D, bottom). Histopathology analyses further revealed a higher number of high-grade melanoma lesions per animal in the *Tet2*$^{lox/lox}$ group than in the *Tet2*$^{+/+}$ group (1.93 vs. 1.17; Fig. 2E). There was also a higher incidence of both locoregional (lymph node) and distant (lung and liver) metastases in *Tet2*$^{lox/lox}$ animals than in *Tet2*$^{+/+}$ mice (on the *Ink4*$^{-/-}$ background; Fig. 2E) as shown on representative pictures of the melanocyte lineage-specific antigen glycoprotein 100 detected by IHC (Fig. 2E, bottom). Altogether, these data indicate that Tet2 depletion favors melanoma initiation and accelerates melanoma progression and metastasis.

Tet2 depletion reduces genome-wide hydroxymethylome plasticity

To gain mechanistic insights into Tet2-mediated tumor suppression, we quantified 5hmC levels in melanoma and control naevi from *Tet2*$^{lox/lox}$ and *Tet2*$^{+/+}$ mice sharing the *Tyr::Cre; Tyr::Nras*^{Q61K}; *Ink4a*$^{-/-}$ genetic background. A significant global decrease in DNA 5hmC, but not 5mC, was detected in melanomas as compared with controls (Fig. 3A; Supplementary Fig. S2). Both control nevi and melanomas from *Tet2*$^{lox/lox}$ mice showed lower global levels of 5hmC than those from *Tet2*$^{+/+}$ mice. Tet2 thus promotes 5-hydroxymethylation in both nevi and melanomas, but it appears not to act alone. Tet1 and Tet3 proteins may also contribute to 5hmC formation in the studied mice, and as Tet1 is

barely detectable in the skin (Supplementary Fig. S2), Tet3 seems likely to play a greater role. It is noteworthy that *Ink4a* depletion alone did not affect global DNA 5hmC levels in nevi samples (Supplementary Fig. S2).

To further dissect the role of Tet2 as a mediator of 5-hydro-xymethylation during melanomagenesis, we applied hMeDIP-seq to biopsies of melanoma tumors (T) and nevi (N) from $Tet2^{lox/lox}$ and $Tet2^{+/+}$ mice sharing the *Tyr::Cre; Tyr::Nras*^{Q61K}; $Ink4a^{-/-}$ background ($n = 2$ or 3 for nevi and $n = 5$ for tumors). Differential analysis revealed only a few regions showing an altered 5hmC content in $Tet2^{lox/lox}$ versus $Tet2^{+/+}$ melanoma biopsies (Fig. 3B; Supplementary Fig. S3). Remarkably, differential hydroxymethylation between melanoma lesions and nevi was far more pronounced in the $Tet2^{+/+}$ samples (Fig. 3B; Supplementary Table S2), and the $Tet2^{+/+}$ tumors predominantly showed a gain rather than a loss.

In $Tet2^{+/+}$ melanoma lesions, differential hydroxymethylation occurred mainly in gene bodies and resulted from both gain and loss of 5hmC (Fig. 3C, left). In contrast, Tet2-depleted melanoma lesions barely showed any enrichment in 5 hmC (Fig. 3C, right; Supplementary Table S3). Overall, only 47 genes were differentially hydroxymethylated in both the $Tet2^{+/+}$ and $Tet2^{lox/lox}$ groups (Fig. 3C). A few DNA regions were chosen randomly from the list of DhmR targets and non-DhmRs of the $Tet2^{+/+}$ groups for validation of the hmedIP-seq. hmC spike-in pull-down followed by qPCR validated the gain or loss of hmC in melanoma tumors as compared with nevi (Supplementary Fig. S3).

These data suggest that the primary function of Tet2 during melanomagenesis is to deposit the 5hmC mark on a selected set of gene bodies. Gene ontology analysis of the genes showing a *Tet2*-dependent increase in 5hmC indicated a significant proportion of genes belonging to the categories “Cancer” (*P* value between 1.56×10^{-3} and 2.7×10^{-62}), “dermatological diseases and conditions” (*P* value between 1.5×10^{-4} and 2.7×10^{-62}), and more strikingly, “nervous system development and function” (*P* value between 1.58×10^{-3} and 7.36×10^{-22}). Using i-cisTarget, an integrative genomic method for predicting of regulatory features and *cis*-regulatory modules (45), we observed a significant overlap between NRSF ChIP-seq tracks and the regions which, in melanomas, show a Tet2-dependent 5hmC gain (NES score: 8.35346). This *in silico* analysis also indicated that these regions contained DNA motifs recognized by FEZ1 (NES score: 4.55114) and Rest/NRSF (NES score: 3.86122). Rest/NRSF is a transcriptional repressor that silences neuronal genes in nonneuronal tissues. It also acts as a key regulator of many neuronal genes, by interacting with Co-rest, Sin3a, and other components of the SWI–SNF chromatin-remodeling complex (46, 47). FEZ1 is required for normal axonal bundling and elongation (48). Thus, the DNA regions showing a Tet2-dependent 5hmC gain in melanomas may be involved in regulating a transcriptional network controlling neuronal/Schwann cell differentiation.

Tet2 depletion reduces gene expression deregulation in melanomas as compared with nevi

To assess the impact of Tet2-mediated gene body hydroxymethylation on gene expression, we analyzed the transcriptomes of a selected group of nevi and melanomas from both $Tet2^{lox/lox}$ and $Tet2^{+/+}$ mice (*Tyr::Cre; Tyr::Nras*^{Q61K}; $Ink4a^{-/-}$). Principal component

analysis of the RNA-seq data revealed a group containing all the melanoma samples ($n = 5$ *Tet2*$^{+/+}$; $n = 5$ *Tet2*$^{lox/lox}$) and a nevus sample group ($n = 4$ *Tet2*$^{+/+}$; $n = 4$ *Tet2*$^{lox/lox}$). Unexpectedly, the samples did not cluster according to the *Tet2* genotype (Fig. 3D). Not a single gene was found to be differentially expressed between *Tet2*$^{lox/lox}$ and *Tet2*$^{+/+}$ nevi (fold change >2; FDR < 0.05), and only 55 genes appeared differentially expressed between *Tet2*$^{lox/lox}$ and *Tet2*$^{+/+}$ melanomas (fold change >2; FDR < 0.05; Supplementary Table S4).

In *Tet2*$^{+/+}$ melanoma lesions, over 7,000 genes showed differential transcript-level expression, mainly downregulation (Fig. 3E; Supplementary Table S2). In the absence of Tet2, the number of dysregulated genes was only slightly above 4,000 (Supplementary Table S3), nearly all of which (3374) were common to the *Tet2*$^{lox/lox}$ and *Tet2*$^{+/+}$ groups and included several melanoma-relevant genes. Deregulated expression of some genes was specifically restricted to samples with one *Tet2* genotype. For example, *Wnt16* and *Wnt5a* (involved, respectively, in senescence and invasion; see refs. 49, 50), showed reduced transcript levels only in *Tet2*$^{+/+}$ melanomas. On the other hand, decreased expression of the genes encoding the *Kdm5d* and *Uty* lysine demethylases and the eukaryotic initiation factor 2 (*Eif2s3y*) was observed only in *Tet2*$^{lox/lox}$ melanomas.

Again, more than a third of the DhmC genes were also differentially expressed (significant overlap, $P = 1.27e{-}50$). Among those overlapping genes, we observed a significative positive correlation ($r = 0.181$; $P = 4.4e{-}5$ and $r = 0.35$; P = 0.026 for *Tet2*$^{+/+}$ group and *Tet2*$^{lox/lox}$ group respectively). Still, only a subset of differentially expressed genes were also differentially hydroxymethylated (Fig. 3F). The transcriptomes of *Tet2*$^{+/+}$ and *Tet2*$^{lox/lox}$ melanomas appeared quite similar with only 55 genes differentially expressed. Hence, one cannot readily explain the phenotype observed in *Tyr::Cre; Tyr::Nras*^{Q61K}; *Tet2*$^{lox/lox}$; *Ink4a*$^{-/-\text{ or }+/-}$ mice on the sole basis of gene expression, and it would seem that Tet2-mediated 5hmC deposition in gene bodies may affect something other than expression of the targeted genes themselves.

Tet2 depletion favors melanocyte expansion in 2D *in vitro* cultures

To gain insights into the mechanisms underpinning Tet2-mediated melanoma suppression, we placed explanted cutaneous melanocytic naevi from *Tet2*$^{+/+}$ and *Tet2*$^{lox/lox}$ mice (i.e., *Tyr::Cre; Tyr::Nras*^{Q61K}; *Ink4a*$^{-/-}$) in 2D culture. Whereas *Tet2*$^{lox/lox}$ cultures divided continuously, *Tet2*$^{+/+}$ control cells ceased to proliferate after only a few passages, adopting a flattened morphology and accumulatingmelanin (Fig. 4A), thus allowing us to perform only a few experiments. *Tet2*$^{lox/lox}$ cultures showed enhanced p-Akt and also expressed higher levels of two known proliferation markers, PCNA and cyclin A, than control *Tet2*$^{+/+}$ cells (Fig. 4B). *Tet2* inactivation thus appears to favor bypass of NRas-induced growth arrest. RT-PCR confirmed that the cells in both cultures produced no *p16*^{Ink4a} transcripts and that, in contrast to the *Tet2*$^{+/+}$ controls, the *Tet2*$^{lox/lox}$ cells did not express *Tet2* (Fig. 4C, where 4T1 breast cancer lines and mES mouse embryonic cell lines were used as additional controls). Interestingly, expression of both *p15/cdkn2b* and *p19/ARF* was dramatically decreased in the cultured *Tet2*$^{lox/lox}$ cells. qRT-PCR analysis also confirmed the melanocytic origin of the cultured cells, as they expressed melanocyte marker genes such as *Tyr, Mitf, S100a6, Pax3*, and *Sox10* (Fig. 4D).

To further explore the role of Tet2 in regulating the *Cdkn2a* locus, we extracted total RNA from tumors dissected from *Tyr::Cre; Tyr::Nras*^{Q61K}; *Ink4a*$^{+/-}$ mice and analyzed expression of the *p16*^{Ink4a} and *p19*^{ARF} genes by qRT-PCR (Fig. 5). Strikingly, decreased *Tet2* gene dosage consistently reduced expression of both *p16* and *p19ARF*. In contrast, expression of *p15/Cdkn2b* and *Pten*, two other melanoma tumor suppressor genes, was unaffected by *Tet2* ablation. Although these data provide some hints about how Tet2 may suppress senescence bypass in preneoplastic lesions, additional experiments will be required to fully explore this potential new function.

Discussion

The aim of the current study was to investigate possible links between the DNA hydroxymethylome and melanoma-genesis. Because human melanomas show disturbed genomes with an altered DNA copy number and high mutational noise, we chose to use a well-established genetically engineered mouse model of melanoma, so as to focus specifically on hydroxymethylome alterations. We provide a detailed analysis of the genomic 5hmC landscape of the widely used mouse model of Nras^{Q61K}-driven melanoma. We also examine the role played by the Tet2 epigenetic factor in countering this disease.

Although a global loss of 5hmC has been described in many cancer types (15, 51), we report here a focal 5hmC gain at discrete loci in cutaneous melanomas, where the 5hmC landscape appears highly remodeled. Although such remodeling has been reported for pancreatic cancer cells (33), it has never been mentioned for melanoma. In contrast to the pancreatic cancer model, we observed in mouse melanomas practically no overlap between genes displaying a 5hmC gain or loss and genes showing altered expression. Although our transcriptomic analysis revealed gene expression alteration and confirmed the deregulation of known melanoma players, only a small subset of genes showing 5hmC changes also appeared affected at transcript level. In that subset, on the basis of the classic view that promoter methylation mediates gene silencing and that 5hmC is a product of demethylation, one might have expected a correlation between changes in 5hmC levels in promoter regions and changes in gene expression. In fact, however, gene expression levels seemed to correlate positively with 5hmC gains in gene bodies. The observation that many of the genes whose expression was altered in melanoma showed no change in 5hmC in their coding regions was not surprising, as not all genes are regulated by DNA methylation. Yet conversely, the transcript level often remained unchanged even when a gene body did show an altered 5hmC content. It is worth noting that An and colleagues (38) likewise observed a poor correlation between TET deletion–related changes in 5mC and gene expression levels. It is imaginable that, rather than directly affecting gene transcription, 5hmC formation or removal might modulate binding of epigenetic factors and result, for instance, in changes in chromatin structure.

By specifically depleting the melanocyte compartment of Tet2, we have shown that Tet2 loss cooperates with mutant NRas to drive melanomagenesis, favoring melanoma initiation and accelerating melanoma progression. As transcriptome analysis revealed only minor differences between tumors expressing Tet2 or not, this effect observed in *Tyr::Cre; Tyr::Nras*^{Q61K}; *Tet2*$^{lox/lox}$; *Ink4a*$^{-/-\text{ or }+/-}$ mice cannot readily be explained on the basis of

gene expression. We have further found Tet2 to be required for hydroxymethylome plasticity during melanomagenesis: most of the gene bodies showing a 5hmC gain in *Tet2*$^{+/+}$ tumors showed no gain in *Tet2*$^{lox/lox}$ tumors. As Tet2-depleted tumors showed practically no focal 5hmC accumulation and developed much earlier than *Tet2*$^{+/+}$ tumors, one might hypothesize that cells use 5hmC enrichment at specific loci as a mechanism counteracting the genesis and/or progression of melanomas as depicted on our hypothetical in Fig. 6. The fact that between *Tet2*$^{lox/lox}$ and *Tet2*$^{+/+}$ tumors we again observed no correlation between 5hmC-level and gene expression changes supports the view that changes in the 5hmC level do not always modulate transcription (52) and that most melanoma-driver genes are not regulated by methylation/hydroxymethylation, although Tet2 might still regulate the expression of some genes via its ability to generate 5hmC. One should also bear in mind that the tumors were collected at an endpoint. We cannot rule out the possibility that a “melanoma transcriptome” might simply be more quickly established in *Tet2*$^{lox/lox}$ than in *Tet2*$^{+/+}$ melanocytes during the early phase of transformation. *Tet2*$^{+/+}$ tumors would thus eventually “catch up” with their *Tet2*$^{lox/lox}$ counterparts. At the level of the hydroxymethylome, Tet2 depletion might likewise allow 5hmC rewriting to occur at an earlier phase of tumor progression, so that endpoint tumors, independently of their *Tet2* genetic status, would resemble each other.

Tet2 loss appears to restrain 5hmC rewriting in tumors. This suggests that 5hmc plasticity might reduce the speed of tumor evolution. In our model, several DNA regions showing specific Tet2-mediated enrichment in 5hmC in melanomas appeared related to neuronal/Schwann cell differentiation. In fact, a population of neural crest cells gives rise to bipotent precursors of Schwann cells and melanocytes. It has been suggested that 5hmC formation and loss of H3K27me3 cooperate to promote brain development (53). The cited study showed that 5hmC associates preferentially with gene bodies of activated neuronal function–related genes. Within these genes, a 5hmC gain was not found to be associated with substantial DNA demethylation and was often accompanied by loss of H3K27me3. Loss or gain of Tet-protein appeared to affect the ability of neural progenitor cells to complete the differentiation process. One might imagine a process in which melanoma cells, while dedifferentiating, would acquire a genome/chromatin conformation more similar to that of neuron/melanocyte (Schwann cell/melanocyte) progenitors. Although these changes would not be sufficient to affect neuronal gene expression or repression, they might constitute a priming event.

Epigenetic mechanisms can affect genome stability (54). Changes in 5hmC patterns might be involved in other cancer-favoring mechanisms, such as genome instability and DNA damage/repair, as recently suggested for bone marrow and spleen cells (29, 38). As mechanisms driving accelerated myeloid leukemo-genesis upon TET loss-of-function, one study pinpointed lineage dysregulation, uncontrolled expansion, and genomic instability in differentiating cells (38). In the case of myeloid malignancies, where the role of Tet2 is more established, work has suggested that *TET2* loss-of-function mutations may precede the acquisition of JAK2V617F mutations in patients with myeloproliferative neoplasms (55). One might likewise imagine that *Tet2* loss favors the acquisition of additional mutations in myeloma-initiating cells, but this must not apply to driver mutations (in *Braf* or *Nras* for instance), because *Tet2*-null mice develop myeloid dysplasia (3) but not melanomas. It is

worth noting that although one might expect cooperation between Tet2 deletion and mutant Braf in melanomagenesis as observed between Tet2 deletion and mutant Nras, additional studies are needed to confirm it. Interestingly, the *Tet2*$^{lox/lox}$ melanocyte line did not express the *cdkn2b* (*p15*) gene, in contrast to its wild-type counterpart. The same applies to the *p19* gene. This suggests a hypothetical explanation for the enhanced capacity of *Tet2*$^{lox/lox}$ melanocytes to divide in culture: As depicted on a hypothetical model (Fig. 6), in the absence of *Ink4a*, depletion of the p15 and p19 cell-cycle inhibitors would allow continuous cell proliferation. Tet2 depletion might thus promote immortalization by preventing transcription of the *p15* and *p19* genes.

Overall, our work highlights the involvement of epigenetic factors in tumor initiation/progression and emphasizes the importance of epigenome plasticity in cancer development (Fig. 6). Although 5hmC is decreased during tumor progression, Tet2-mediated maintenance of 5hmC at specific target sites may delay this progression or prevent loss of cell identity.

Supplementary Material

Refer to Web version on PubMed Central for supplementary material.

Acknowledgments

We thank G. Bervoets for technical assistance and F. Rambow for helpful discussions. E. Bonvin was supported by the Belgian Fonds de la Recherche Scientifique (FNRS). M. Bizet was supported by a Télévie grant. F. Fuks is a ULB Full Professor and his lab is funded by grants from the FNRS and Télévie, the Interuniversity Attraction Poles (P7/03) program, the Action de Recherche Concertée (ARC; AUWB-2010–2015 ULB-No 7), the Belgian "Fondation contre le Cancer" (FCC 2016–086 FAF-F/2016/872), and the Fonds Gaston Ithier. S. Santagostino was supported in part by NIH/NCI Cancer Center Support Grant P30 CA008748.

The costs of publication of this article were defrayed in part by the payment of page charges. This article must therefore be hereby marked *advertisement* in accordance with 18 U.S.C. Section 1734 solely to indicate this fact.

References

1. Delatte B, Deplus R, Fuks F. Playing TETris with DNA modifications. EMBO J 2014;33:1198–211. [PubMed: 24825349]
2. Li Z, Cai X, Cai C-L, Wang J, Zhang W, Petersen BE, et al. Deletion of Tet2 in mice leads to dysregulated hematopoietic stem cells and subsequent development of myeloid malignancies. Blood 2011;118:4509–18. [PubMed: 21803851]
3. Moran-Crusio K, Reavie L, Shih A, Abdel-Wahab O, Ndiaye-Lobry D, Lobry C, et al. Tet2 loss leads to increased hematopoietic stem cell self-renewal and myeloid transformation. Cancer Cell 2011;20:11–24. [PubMed: 21723200]
4. Costa Y, Ding J, Theunissen TW, Faiola F, Hore TA, Shliaha PV.et al. NANOG-dependent function of TET1 and TET2 in establishment of pluripotency. Nature 2013;495:370–4. [PubMed: 23395962]
5. Huang Y, Chavez L, Chang X, Wang X, Pastor WA, Kang J, et al. Distinct roles of the methylcytosine oxidases Tet1 and Tet2 in mouse embryonic stem cells. Proc Natl Acad Sci U S A 2014;111:1361–6. [PubMed: 24474761]
6. Ghosh P, Chin L. Genetics and genomics of melanoma. Expert Rev Dermatol 2009;4:131. [PubMed: 20126509]
7. Jin S-G, Xiong W, Wu X, Yang L, Pfeifer GP. The DNA methylation landscape of human melanoma. Genomics 2015;106:322–30. [PubMed: 26384656]

8. Mologhoni F, Cruz AT, Meliso FM, Morais AS, Souza CF, Xander P, et al. Epigenetic reprogramming as a key contributor to melanocyte malignant transformation. Epigenetics 2014;6:450–64.
9. Zingg D, Debbache J, Schaefer SM, Tuncer E, Frommel SC, Cheng P, et al. The epigenetic modifier EZH2 controls melanoma growth and metastasis through silencing of distinct tumour suppressors. Nat Commun 2015;6: 6051. [PubMed: 25609585]
10. Mirmohammadsadegh A, Marini A, Nambiar S, Hassan M, Tannapfel A, Ruzicka T, et al. Epigenetic silencing of the PTEN gene in melanoma. Cancer Res 2006;66:6546–52. [PubMed: 16818626]
11. Jonsson A, Tuominen R, Grafström E, Hansson J, Egyhazi S. High frequency of p16INK4A promoter methylation in NRAS-mutated cutaneous melanoma. J Invest Dermatol 2010;130:2809–17. [PubMed: 20703244]
12. Fiziev P, Akdemir KC, Miller JP, Keung EZ, Samant NS, Sharma S, et al. Systematic epigenomic analysis reveals chromatin states associated with melanoma progression. Cell Rep 2017;19:875–89. [PubMed: 28445736]
13. Gambichler T, Sand M, Skrygan M. Loss of 5-hydroxymethylcytosine and ten-eleven translocation 2 protein expression in malignant melanoma. Melanoma Res 2013;23:218–20. [PubMed: 23458759]
14. Lian CG, Xu Y, Ceol C, Wu F, Larson A, Dresser K, et al. Loss of 5-hydroxymethylcytosine is an epigenetic hallmark of melanoma. Cell 2012;150: 1135–46. [PubMed: 22980977]
15. Gao J, Aksoy BA, Dogrusoz U, Dresdner G, Gross B, Sumer SO, et al. Integrative analysis of complex cancer genomics and clinical profiles using the cBioPortal. Sci Signal 2013;6:pl1. [PubMed: 23550210]
16. Cerami E, Gao J, Dogrusoz U, Gross BE, Sumer SO, Aksoy BA, et al. The cBio Cancer Genomics Portal: An Open Platform for Exploring Multidimensional Cancer Genomics Data: Figure 1. Cancer Discov 2012;2:401–4. [PubMed: 22588877]
17. Delmas V, Martinozzi S, Bourgeois Y, Holzenberger M, Larue L. Cre-mediated recombination in the skin melanocyte lineage. Genesis 2003; 36:73–80. [PubMed: 12820167]
18. Serrano M, Lee H, Chin L, Cordon-Cardo C, Beach D, DePinho RA. Role of the INK4a locus in tumor suppression and cell mortality. Cell 1996;85: 27–37. [PubMed: 8620534]
19. Ackermann J, Frutschi M, Kaloulis K, Qk AN, Background I, Mckee T, et al. Metastasizing melanoma formation caused by expression of activated N-RasQ61K on an INK4a-deficient background. Cancer Res 2005;65: 4005–11. [PubMed: 15899789]
20. Gross A, Ziepert M, Scholz M, Nickelsen M, Ho A. KMWin – a convenient tool for graphical presentation of results from Kaplan-Meier survival time analysis. PLoS One 2012;7:e38960. [PubMed: 22723912]
21. Campagne C, Reyes-Gomez E, Battistella M, Bernex F, Château-Joubert S, Huet H, et al. Histopathological atlas and proposed classification for melanocytic lesions in Tyr::NRas(Q61K); Cdkn2a(−/−) transgenic mice. Pigment Cell Melanoma Res 2013;26:735–42. [PubMed: 23647911]
22. Li H, Durbin R. Fast and accurate long-read alignment with Burrows–Wheeler transform. Bioinformatics 2010;26:589–95. [PubMed: 20080505]
23. Liao Y, Smyth GK, Shi W. featureCounts: an efficient general purpose program for assigning sequence reads to genomic features. Bioinformatics 2014;30:923–30. [PubMed: 24227677]
24. Robinson MD, McCarthy DJ, Smyth GK. edgeR: a Bioconductor package for differential expression analysis of digital gene expression data. Bioinformatics 2010;26:139–40. [PubMed: 19910308]
25. Visel A, Minovitsky S, Dubchak I, Pennacchio LA. VISTA Enhancer Browser–a database of tissue-specific human enhancers. Nucleic Acids Res 2007;35:D88–92. [PubMed: 17130149]
26. Quinlan AR. BEDTools: The Swiss-Army Tool for Genome Feature Analysis. Curr Protoc Bioinforma 2014;47:11.12.1–34.
27. Dobin A, Davis CA, Schlesinger F, Drenkow J, Zaleski C, Jha S, et al. STAR: ultrafast universal RNA-seq aligner. Bioinformatics 2013;29:15–21. [PubMed: 23104886]
28. Anders S, Pyl PT, Huber W. HTSeq–a Python framework to work with high-throughput sequencing data. Bioinformatics 2015;31:166–9. [PubMed: 25260700]

29. Kim D, Pertea G, Trapnell C, Pimentel H, Kelley R, Salzberg SL, et al. TopHat2: accurate alignment of transcriptomes in the presence of insertions, deletions and gene fusions. Genome Biol 2013;14:R36. [PubMed: 23618408]
30. Ackermann J, Frutschi M, Kaloulis K, McKee T, Trumpp A, Beermann F. Metastasizing melanoma formation caused by expression of activated N-RasQ61K on an INK4a-deficient background. Cancer Res 2005;65: 4005–11. [PubMed: 15899789]
31. Olvedy M, Tisserand JC, Luciani F, Boeckx B, Wouters J, Lopez S, et al. Comparative oncogenomics identifies tyrosine kinase FES as a tumor suppressor in melanoma. J Clin Invest 2017;127:2310–25. [PubMed: 28463229]
32. Song C-X, Szulwach KE, Fu Y, Dai Q, Yi C, Li X, et al. Selective chemical labeling reveals the genome-wide distribution of 5-hydroxymethylcytosine. Nat Biotechnol 2011;29:68–72. [PubMed: 21151123]
33. Bhattacharyya S, Yu Y, Suzuki M, Campbell N, Mazdo J, Vasanthakumar A, et al. Genome-wide hydroxymethylation tested using the HELP-GT assay shows redistribution in cancer. Nucleic Acids Res 2013;41:e157. [PubMed: 23861445]
34. Schliekelman MJ, Gibbons DL, Faca VM, Creighton CJ, Rizvi ZH, Zhang Q, et al. Targets of the tumor suppressor miR-200 in regulation of the epithelial-mesenchymal transition in cancer. Cancer Res 2011;71: 7670–82. [PubMed: 21987723]
35. Kwong LN, Zou L, Chagani S, Zhang J, Pedamallu CS, Liu M, et al. Modeling genomic instability and selection pressure in a mouse model of melanoma. Cell Rep 2017;19:1304–12. [PubMed: 28514651]
36. Cheung AF, Dupage MJP, Dong HK, Chen J, Jacks T. Regulated expression of a tumor-associated antigen reveals multiple levels of T-cell tolerance in a mouse model of lung cancer. Cancer Res 2008;68:9459–68. [PubMed: 19010921]
37. Smith AP, Hoek K, Becker D. Whole-genome expression profiling of the melanoma progression pathway reveals marked molecular differences between nevi/melanoma in situ and advanced-stage melanomas. Cancer Biol Ther 2005;4:1018–29. [PubMed: 16251803]
38. An J, González-Avalos E, Chawla A, Jeong M, López-Moyado IF, Li W, et al. Acute loss of TET function results in aggressive myeloid cancer in mice. Nat Commun 2015;6:10071. [PubMed: 26607761]
39. Tan L, Xiong L, Xu W, Wu F, Huang N, Xu Y, et al. Genome-wide comparison of DNA hydroxymethylation in mouse embryonic stem cells and neural progenitor cells by a new comparative hMeDIP-seq method. Nucleic Acids Res 2013;41:e84. [PubMed: 23408859]
40. Nestor CE, Ottaviano R, Reddington J, Sproul D, Reinhardt D, Dunican D, et al. Tissue type is a major modifier of the 5-hydroxymethylcytosine content of human genes. Genome Res 2012;22:467–77. [PubMed: 22106369]
41. Nestor CE, Ottaviano R, Reinhardt D, Cruickshanks HA, Mjoseng HK, McPherson RC, et al. Rapid reprogramming of epigenetic and transcriptional profiles in mammalian culture systems. Genome Biol 2015;16:11. [PubMed: 25648825]
42. Xu Y, Wu F, Tan L, Kong L, Xiong L, Deng J, et al. Genome-wide regulation of 5hmC, 5mC, and gene expression by Tet1 hydroxylase in mouse embryonic stem cells. Mol Cell 2011;42:451–64. [PubMed: 21514197]
43. Delmas V, Beermann F, Martinozzi S, Carreira S, Ackermann J, Kumasaka M, et al. beta-Catenin induces immortalization of melanocytes by suppressing p16INK4a expression and cooperates with N-Ras in melanoma development. Genes Dev 2007;21:2923–35. [PubMed: 18006687]
44. Shakhova O, Zingg D, Schaefer SM, Hari L, Civenni G, Blunschi J, et al. Sox10 promotes the formation and maintenance of giant congenital naevi and melanoma. Nat Cell Biol 2012;14:882–90. [PubMed: 22772081]
45. Herrmann C, Van de Sande B, Potier D, Aerts S. i-cisTarget: an integrative genomics method for the prediction of regulatory features and cis-regulatory modules. Nucleic Acids Res 2012;40:e114. [PubMed: 22718975]
46. Battaglioli E, Andrés ME, Rose DW, Chenoweth JG, Rosenfeld MG, Anderson ME, et al. REST repression of neuronal genes requires components of the hSWI.SNF complex. J Biol Chem 2002;277:41038–45. [PubMed: 12192000]

47. Sun Y-M, Greenway DJ, Johnson R, Street M, Belyaev ND, Deuchars J, et al. Distinct profiles of REST interactions with its target genes at different stages of neuronal development. Mol Biol Cell 2005;16:5630–8. [PubMed: 16195345]

48. Kuroda S, Nakagawa N, Tokunaga C, Tatematsu K, Tanizawa K. Mammalian homologue of the Caenorhabditis elegans UNC-76 protein involved in axonal outgrowth is a protein kinase C zeta-interacting protein. J Cell Biol 1999;144:403–11. [PubMed: 9971736]

49. Binet R, Ythier D, Robles AI, Collado M, Larrieu D, Fonti C, et al. Cell, tumor, and stem cell biology WNT16B is a new marker of cellular senescence that regulates p53 activity and the phosphoinositide 3-kinase/AKT pathway. Cancer Res 2009;69:9183–91. [PubMed: 19951988]

50. Webster MR, Xu M, Kinzler KA, Kaur A, Appleton J, O'Connell MP, et al. Wnt5A promotes an adaptive, senescent-like stress response, while continuing to drive invasion in melanoma cells. Pigment Cell Melanoma Res 2015;28:184–95. [PubMed: 25407936]

51. Jin S-G, Jiang Y, Qiu R, Rauch TA, Wang Y, Schackert G, et al. 5-Hydroxymethylcytosine is strongly depleted in human cancers but its levels do not correlate with IDH1 mutations. Cancer Res 2011;71: 7360–5. [PubMed: 22052461]

52. Wu D, Hu D, Chen H, Shi G, Fetahu IS, Wu F, et al. Glucose-regulated phosphorylation of TET2 by AMPK reveals a pathway linking diabetes to cancer. Nature 2018;559:637–41. [PubMed: 30022161]

53. Hahn MA, Qiu R, Wu X, Li AX, Zhang H, Wang J, et al. Dynamics of 5-hydroxymethylcytosine and chromatin marks in mammalian neurogenesis. Cell Rep 2013;3:291–300. [PubMed: 23403289]

54. Putiri EL, Robertson KD. Epigenetic mechanisms and genome stability. Clin Epigenetics 2010;2:299–314.

55. Haeno H, Levine RL, Gilliland DG, Michor F. A progenitor cell origin of myeloid malignancies. Proc Natl Acad Sci U S A 2009;106:16616–21. [PubMed: 19805346]

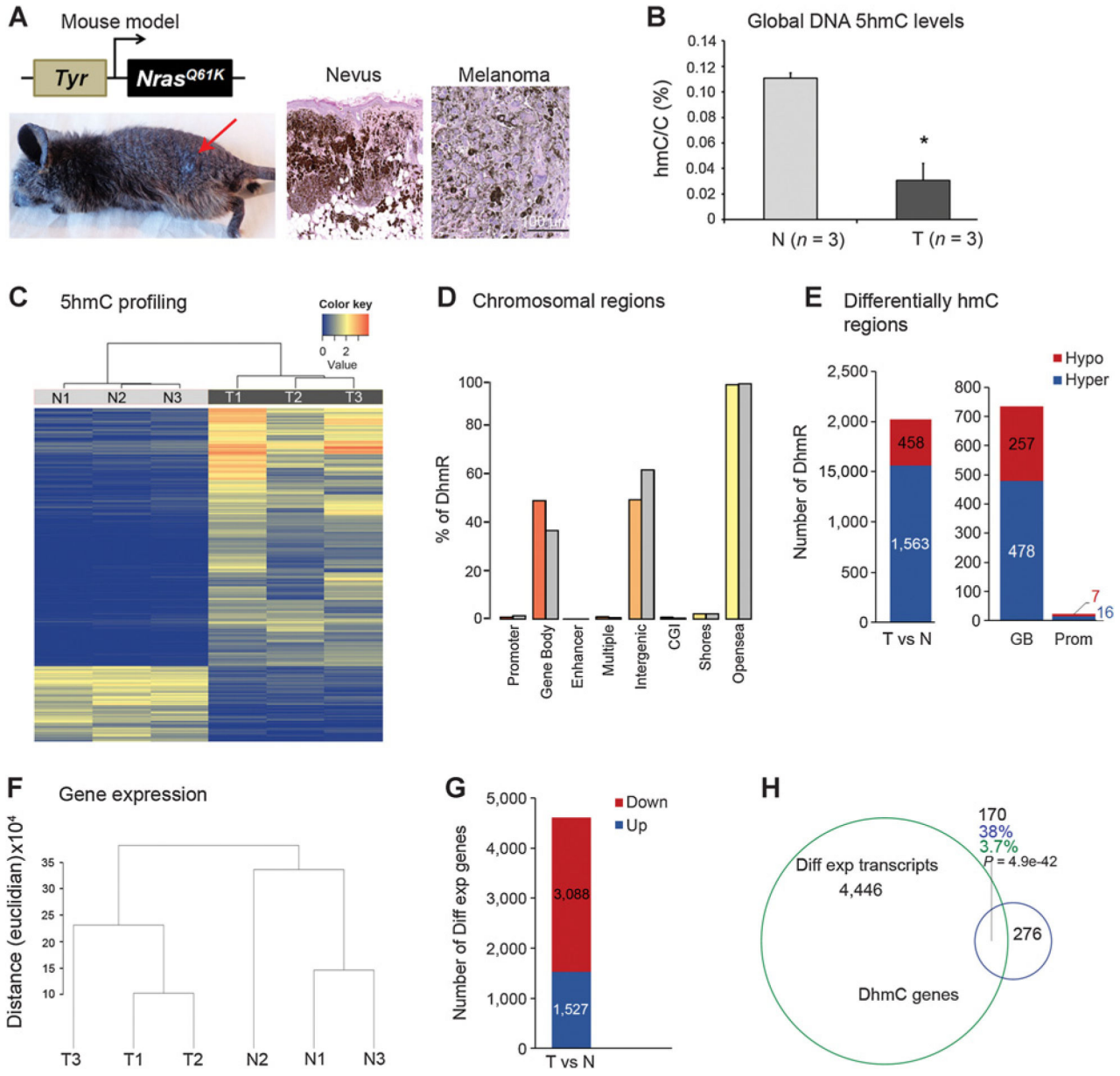

Figure 1.

Global and local changes in DNA 5hmC in a murine model of melanoma. **A**, Schematic representation of the transgene. Mice expressing the *Nras* oncogene are hyperpigmented (nevus-like) and develop melanoma (left, photo of a mouse bearing a skin melanoma; right, H&E of skin and melanoma sections). **B**, Global DNA 5hmC content of melanoma tumours (T; $n = 3$) and control nevi (N; $n = 3$), measured by mass spectrometry. Data, means±SD. Statistical evaluation with Student unpaired two-tailed t test gave $P = 0.003$ indicated by *. **C**, Hierarchical clustering of nevi and melanoma samples based on 5hmC-containing DNA regions (nevi $n = 3$, tumors $n = 3$). **D**, Proportional distribution of differentially hydroxymethylated regions (DhmR) along the genome (color bars) compared with expected (gray). **E**, Numbers of differentially hydroxymethylated regions (hypo or hyper) and their localization (prom, promoter; GB, gene body). **F**, Hierarchical clustering based on the

expression of genes determined by RNA-seq. **G**, Number of transcripts showing statistically differential expression between melanoma tumors (T) and nevi (N). **H**, Area-proportional Venn diagram representation of DhmR and differentially expressed genes.

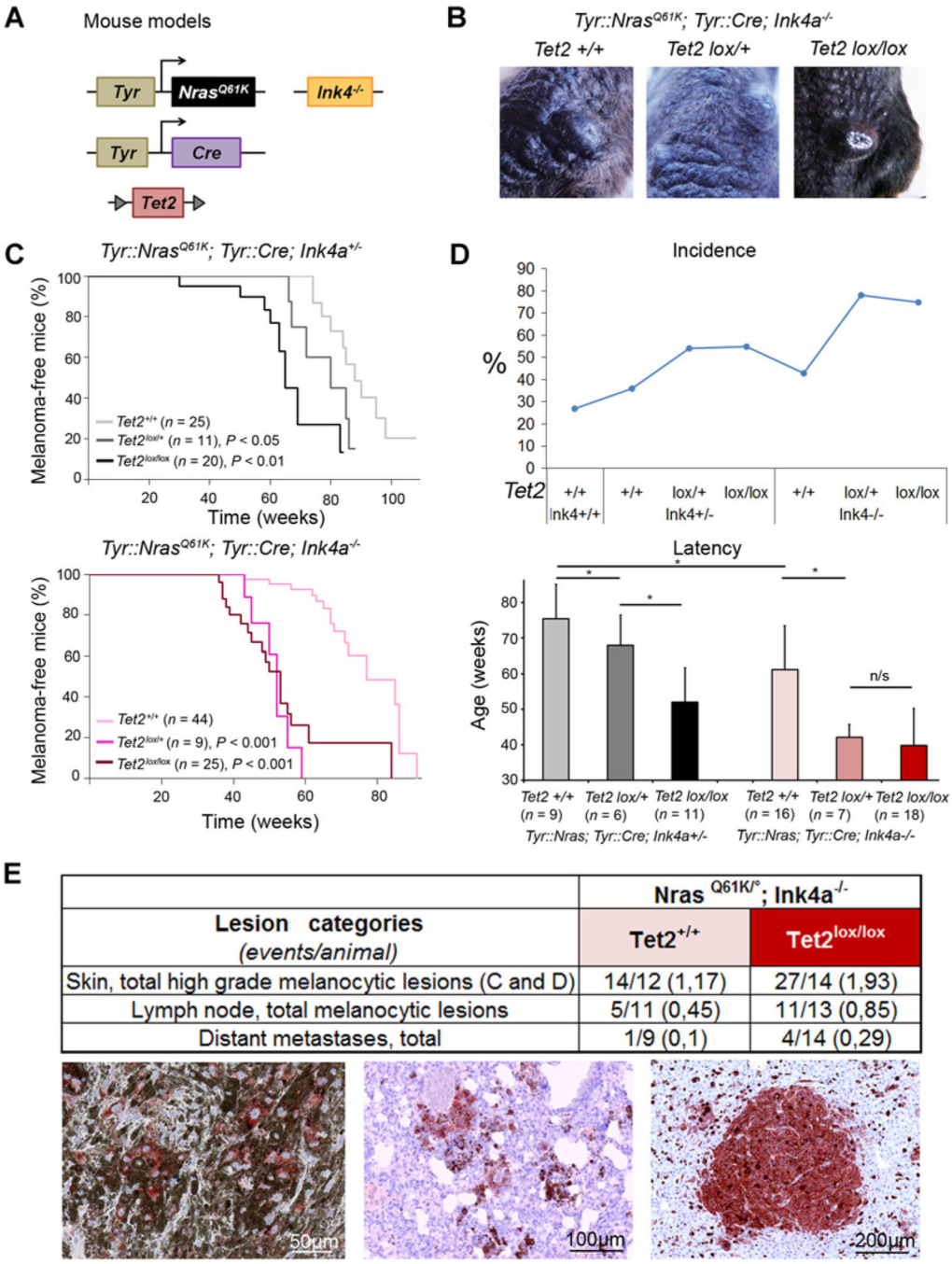

Lesion categories (events/animal)	Nras $^{Q61K/°}$; Ink4a$^{-/-}$ Tet2$^{+/+}$	Nras $^{Q61K/°}$; Ink4a$^{-/-}$ Tet2$^{lox/lox}$
Skin, total high grade melanocytic lesions (C and D)	14/12 (1,17)	27/14 (1,93)
Lymph node, total melanocytic lesions	5/11 (0,45)	11/13 (0,85)
Distant metastases, total	1/9 (0,1)	4/14 (0,29)

Figure 2.

Tet2 loss cooperates with oncogenic NRas and p16^{Ink4a} depletion to generate melanoma in mice. **A**, Schematic representation of the transgenes. The *Nras* oncogene is expressed and *Tet2* expression is abolished in the melanocyte lineage of mice with the *Ink4a*$^{+/-}$ or *Ink4a*$^{-/-}$ background. **B**, Identification of tumor-bearing mice by visual inspection. In mice expressing oncogenic *Nras* and not *Ink4a*, independently of the *Tet2* genetic status, melanomas appeared mainly on the back. **C**, Tumor-free survival curves are shown for the effect of Tet2 depletion in Nras-oncogene–expressing *Ink4a*$^{+/-}$ (top) and *Ink4a*$^{-/-}$ mice

(bottom). *P* values resulting from the log-rank test indicated statistically significant difference as compared with *Tet2*$^{+/+}$ controls. In mice with the *Ink4a*$^{+/-}$ background, melanoma-free survival differed significantly between *Tet2*$^{lox/lox}$ and *Tet2*$^{lox/+}$ mice, $P < 0.05$. This was not the case of mice with the *Ink4a*$^{-/-}$ background. **D**, Graph of incidence indicating the proportions of Nras-mutant mice developing a C or D skin lesion (top) and graph indicating the average time of tumor appearance for each genotype (bottom). *t* test resulting *P* values are indicated as * when <0.05. n/s, nonsignificant. **E**, Anatomo-histologic analysis of samples showing that *Tet2* deficiency leads to an increased number of events (type-C or -D skin lesions and metastases) per animal having the *Nras*^{Q61K}; *Ink4a*$^{-/-}$ background (top). Representative IHC images of gp100 are shown and scale bars are indicated at the bottom right of each picture: subcutis type-D lesion (left), lung metastasis (middle), and liver metastasis (bottom right).

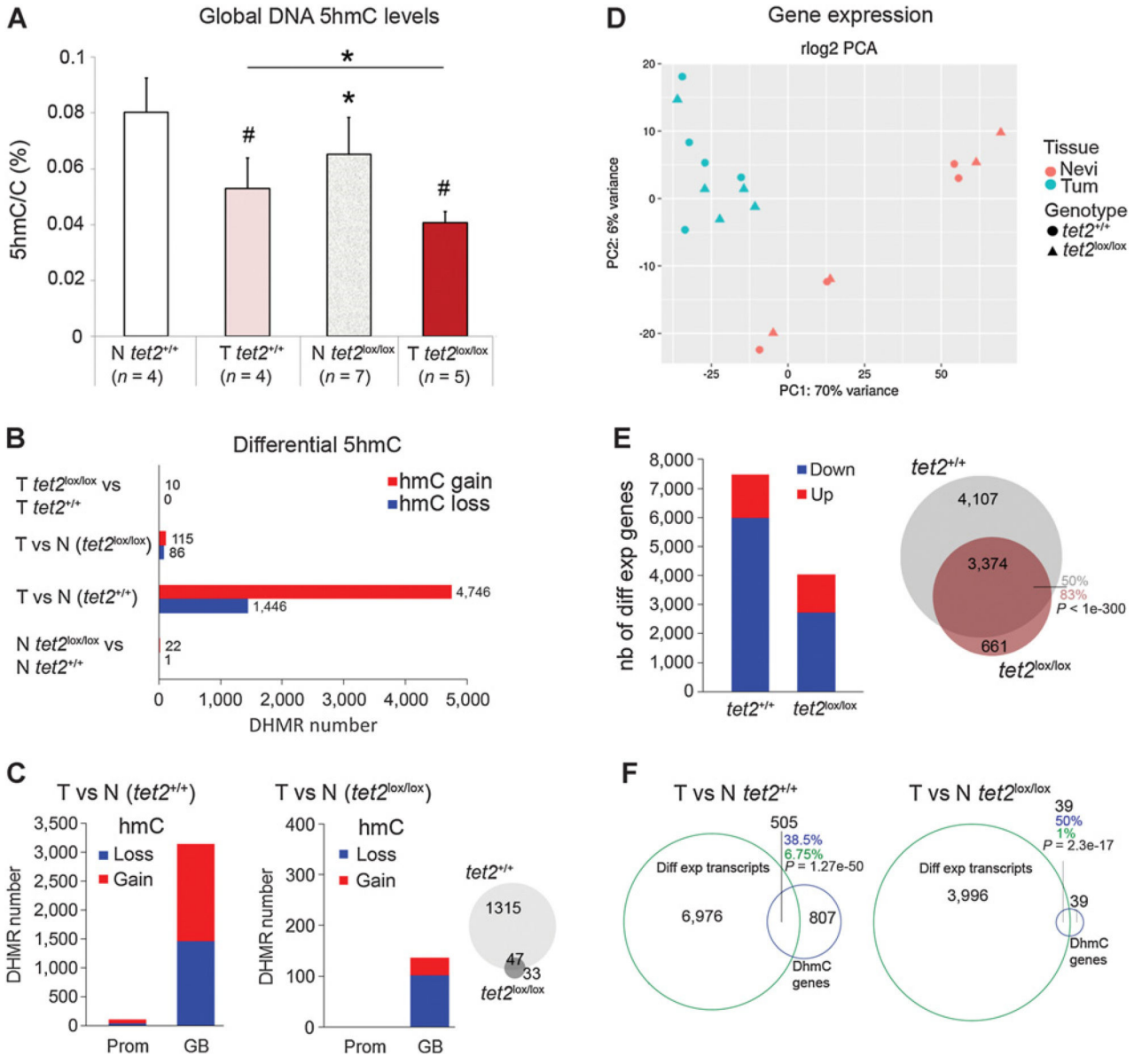

Figure 3.

Tet2 depletion reduces hydroxymethylome plasticity in melanoma on *Tyr::Nras*^{Q61K}; *Ink4a*$^{-/-}$ background. **A**, Global DNA 5hmC content measured by mass spectrometry in biopsies of melanoma tumors (T) and control nevi (N) from *Tyr::Nras*^{Q61K}; *Tyr::Cre; Ink4a*$^{-/-}$; *Tet2*$^{+/+}$ or *Tet2*$^{lox/lox}$ mice. #, P < 0.005; *, P < 0.05. **B**, hMedIP-seq data showing differentially hydroxymethylated regions for a set of 4 comparisons. **C**, The graphs show the number of genic regions displaying either a gain or a loss of 5hmC in tumors as compared to nevi of *Tet2*$^{+/+}$ (left) and *Tet2*$^{lox/lox}$ mice (right) sharing the *Tyr::Nras*^{Q61K}; *Tyr::Cre; Ink4a*$^{-/-}$ background. **D**, Principal component analysis of RNA-seq data shows two clusters (melanoma tumors in blue and nevi in red) but fails to distinguish samples according to the *Tet2* genetic status. Nevi *n* = 4, tumors *n* = 5 for each group. **E**, Bar plot representation of genes showing a statistically significant difference in gene expression (fold change > 2; FRD

< 0.05) between tumors and nevi having either the *Tet2*$^{+/+}$ or the *Tet2*$^{lox/lox}$ genotype (left). Area-proportional Venn diagram representation of genes differentially expressed in melanomas versus nevi. **F**, Area-proportional Venn diagram representation of DhmRs and differentially expressed genes between tumors and nevi for the *Tet2*$^{+/+}$ and *Tet2*$^{lox/lox}$ groups.

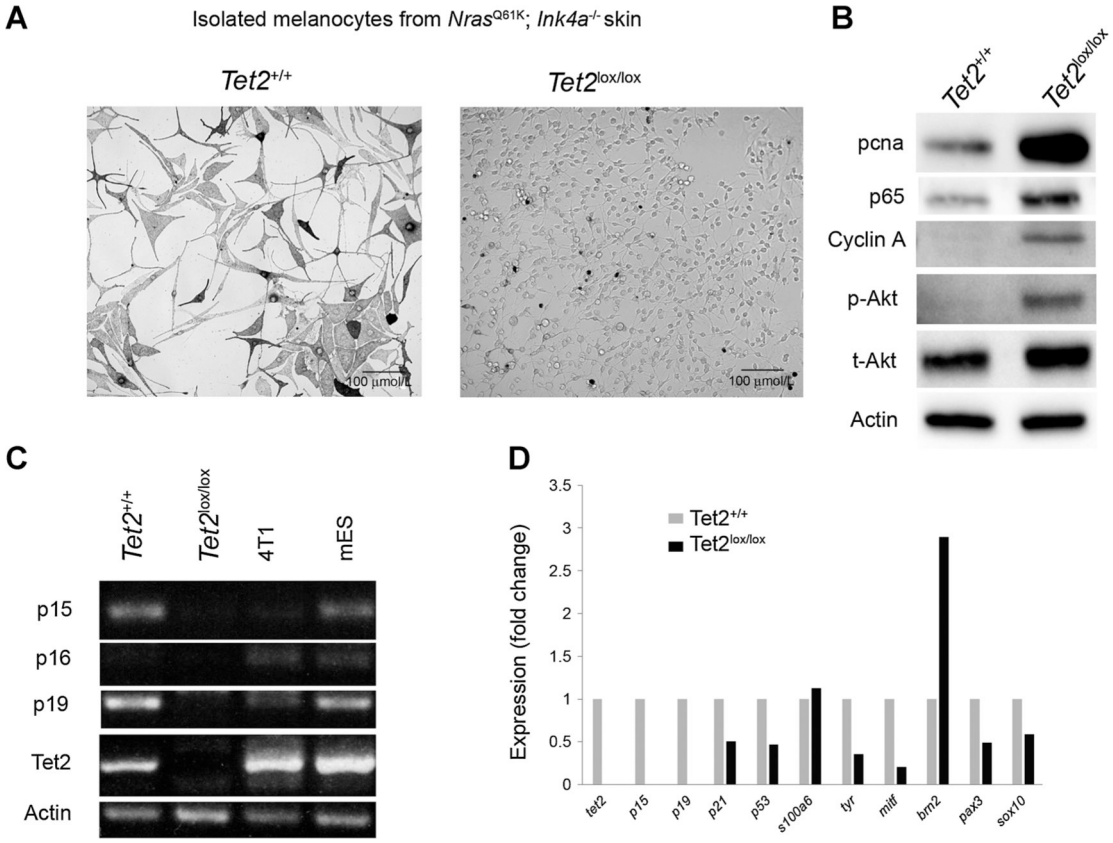

Figure 4.

Isolated *Tet2*$^{+/+}$ and *Tet2*$^{lox/lox}$ melanocytes show different morphologies and abilities to grow *in vitro*. **A**, Picture showing the gross morphology of melanocytes isolated from *Tet2*$^{+/+}$ *and Tet2*$^{lox/lox}$ mice sharing the *Tyr::Nras*^{Q61K}; *Tyr::Cre; Ink4a*$^{-/-}$ background, $n = 1$ for each genotype. **B**, Western blot analysis of isolated and cultured melanocytes shows enhanced levels of proliferation-related proteins (Pcna and cyclin A) and Akt-pathway proteins, specifically in *Tet2*$^{lox/lox}$ cells. **C**, RT-PCR–based analysis of gene expression of four cell types. Unrelated cell types as controls: the 4T1 murine breast cancer cell line and mouse embryonic stem cells (mESC). Expression of cell-cycle inhibitor genes is lost in *Tet2*$^{lox/lox}$ cells as compared with *Tet2*$^{+/+}$ cells. **D**, qRT-PCR analysis of cell-cycle gene and melanocyte marker gene expression.

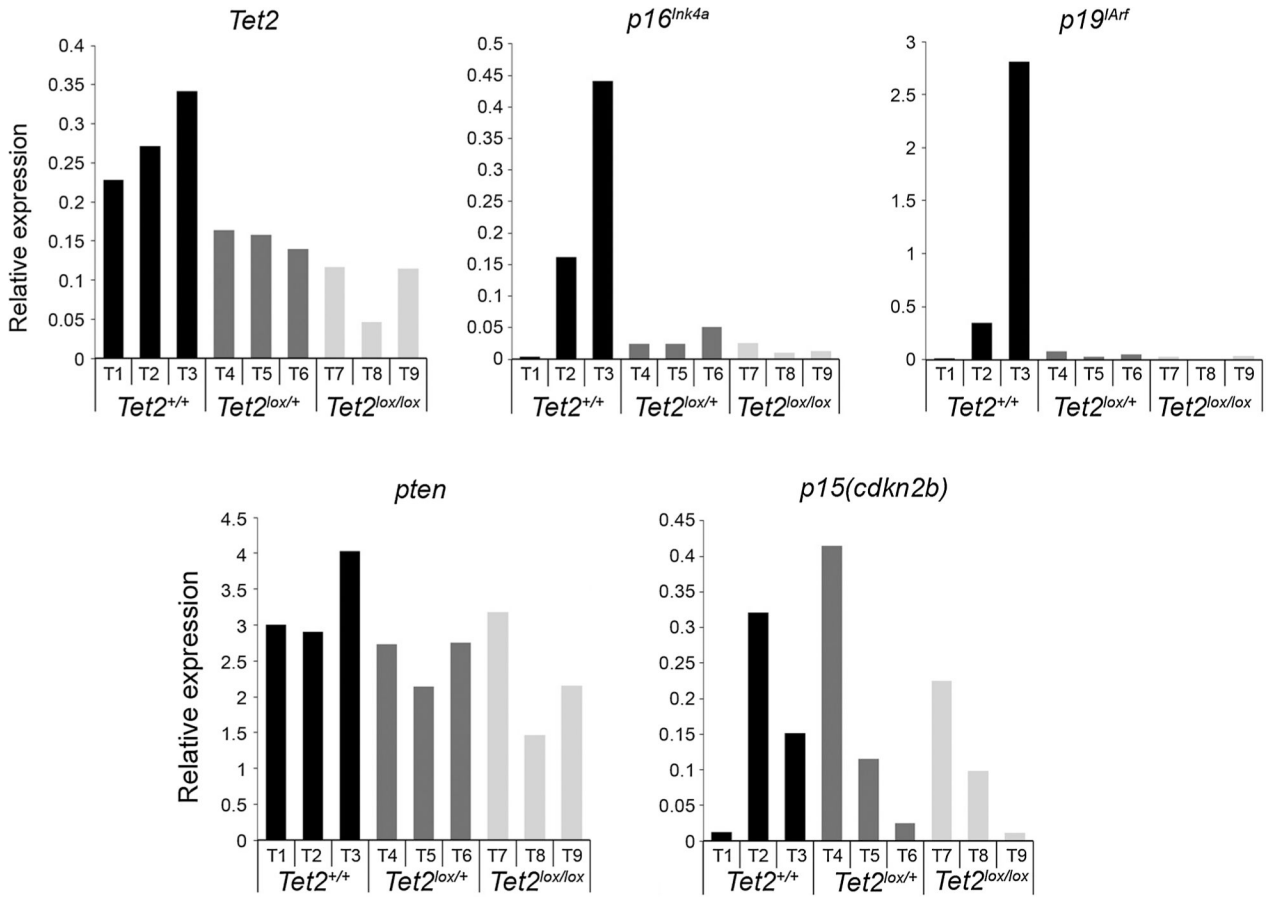

Figure 5.

Tet2 depletion tends to favor *ink4a* loss of expression. qRT-PCR analysis of *Tet2* and cell-cycle inhibitor gene transcripts performed on melanoma biopsies from $Tet2^{+/+}$, $Tet2^{lox/+}$, and $Tet2^{lox/lox}$ mice sharing the $Tyr::Nras^{Q61K/°}$; *Tyr::Cre;* $Ink4a^{+/-}$ background. The *Hprt* housekeeping gene was used for normalization.

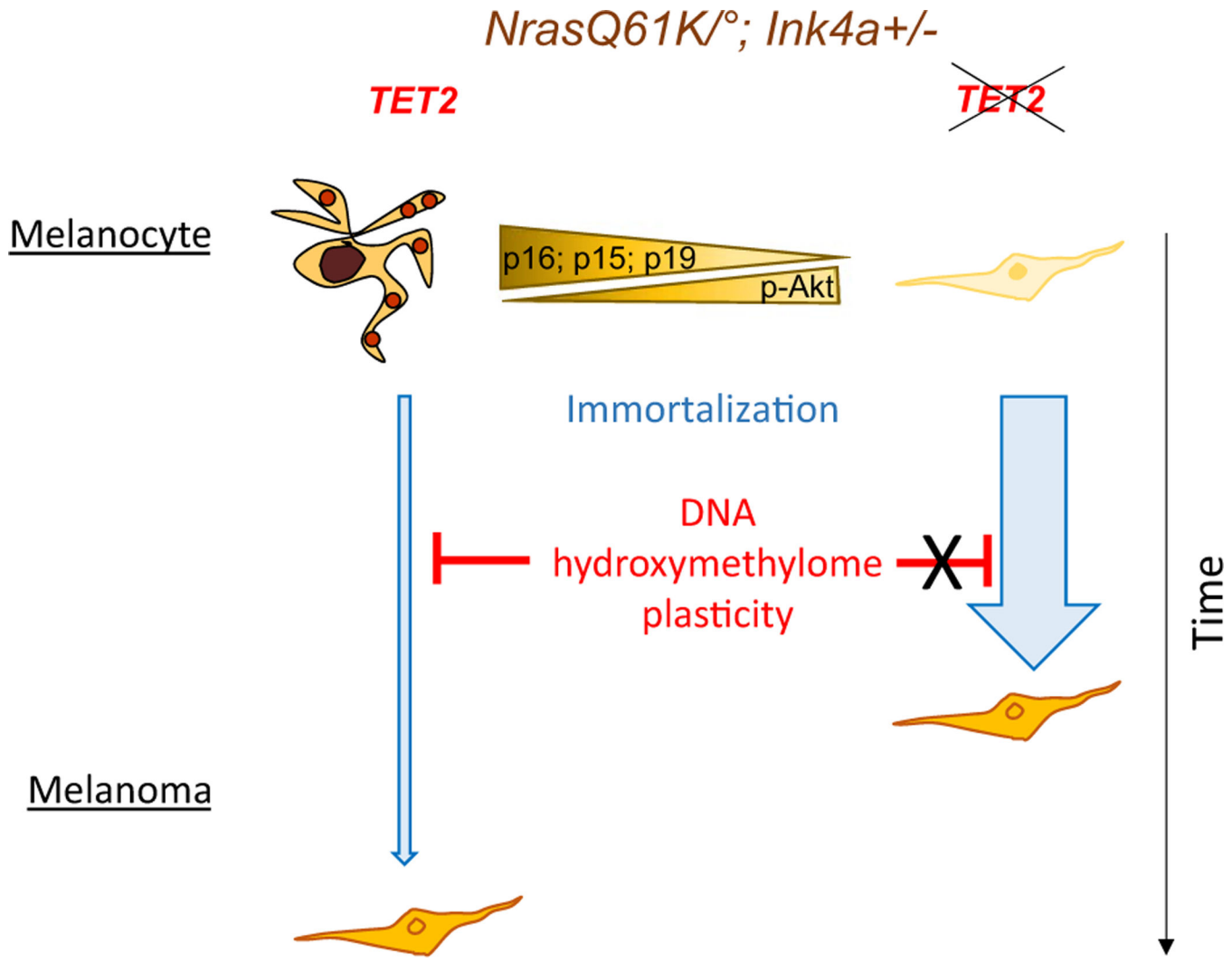

Figure 6.

Hypothetical model. *Tet2* depletion together with *Nras* mutation increase melanoma incidence and reduces the latency. In cooperation with Nras activation, *Tet2* depletion would favor cell immortalization and facilitate melanoma emergence by (i) reducing cell-cycle inhibitor/tumor suppressor expression; (ii) allowing Akt activation, and (iii) reducing the hydroxymethylome plasticity, a bunch of phenomena that influence tumor homeostasis.